# Frequency Spectra and the Color of Cellular Noise

Ankit Gupta and Mustafa Khammash
Department of Biosystems Science and Engineering
ETH Zurich
Mattenstrasse 26
4058 Basel, Switzerland.

September 16, 2020

**Abstract**

The invention of the Fourier integral in the 19th century laid the foundation for modern spectral analysis methods. By decomposing a (time) signal into its essential frequency components, these methods uncovered deep insights into the signal and its generating process, precipitating tremendous inventions and discoveries in many fields of engineering, technology, and physical science. In systems and synthetic biology, however, the impact of frequency methods has been far more limited despite their huge promise. This is in large part due to the difficulty of gleaning spectral information from single-cell trajectories, owing to their distinctive noisy character forged by the underlying discrete stochastic dynamics of the living cell, typically modelled as a continuous-time Markov chain (CTMC). Here we draw on stochastic process theory to develop a spectral theory and computational methodologies tailored specifically to the computation and analysis of frequency spectra of noisy cellular networks. For linear networks we present exact expressions for the frequency spectrum and use them to decompose the variability of a signal into its sources. For nonlinear networks, we develop methods to obtain accurate Padé approximants of the spectrum from a single Monte Carlo trajectory simulation. Our results provide new conceptual and practical methods for the analysis and design of noisy cellular networks based on their output frequency spectra. We illustrate this through diverse case studies in which we show that the single-cell frequency spectrum enables topology discrimination, synthetic oscillator optimization, cybergenetic controller design, and systematic investigation of stochastic entrainment.

Keywords: Power Spectral Density; Frequency Spectrum; Stochastic Reaction Networks; Time Lapse Microscopy; Systems Biology; Synthetic Biology

## 1 Introduction

Modern microscopy and the advent of a wide array of fluorescent protein has afforded scientists the unprecedented ability to monitor the dynamics of living biological cells [57]. The rapid pace of development in imaging technology coupled with advanced image processing techniques has made it viable to obtain high-resolution time-lapse live-cell data for a multitude of cell-types and biological processes [67]. However theoretical and computational tools for quantitatively extracting information about intracellular networks from such data are still underdeveloped. One of the main reasons why the development of these tools is mathematically challenging is that the dynamics of single-cells is inherently noisy due to randomness in molecular interactions that constitute intracellular processes, and hence single-cell dynamics must be described with stochastic models that are more difficult to analyse than their deterministic counterparts [36]. These stochastic models usually represent the reaction dynamics as a continuous-time Markov chain (CTMC) and the existing methods for analysing them have mostly focussed on solving the Chemical Master Equation (CME) that governs the evolution of the probability distribution of the random state [2]. While these methods have been successfully applied in several significant biological studies [54, 6], they typically do not account for temporal correlations in time-traces of living cells, but rather they are designed to connect network models to flow-cytometry data [31] where temporal correlations are anyway lost due to discarding of the measured cells. Temporal correlations are a feature of single-cell trajectories that contain valuable

**Box 1: Frequency domain analysis of stochastic signals**

Consider a reaction network, comprising species $\mathbf{X}_1, \ldots, \mathbf{X}_d$ whose copy-number dynamics is described by an ergodic *continuous-time Markov chain* (CTMC) $(X(t))_{t\geq 0}$ with stationary distribution $\pi$. Our goal is to estimate the PSD which measures the strengths of oscillatory components of various frequencies in the output signal $(X_n(t))_{t\geq 0}$ tracking the copy-number trajectory for species $\mathbf{X}_n$. We first subtract the stationary mean $\mathbb{E}_\pi(X_n)$ and construct the mean zero signal as $\widetilde{X}_n(t) = X_n(t) - \mathbb{E}_\pi(X_n)$ and then the time-averaged signal power $P(X_n)$ is equal to the stationary variance $\mathrm{Var}_\pi(X_n)$, i.e.

$$P(X_n) := \lim_{T\to\infty} T^{-1} \int_0^T \left(\widetilde{X}_n(t)\right)^2 dt = \mathrm{Var}_\pi(X_n).$$

The *power spectral density (PSD)* for the output signal is given by

$$S_{X_n}(\omega) = \lim_{T\to\infty} T^{-1} |\mathcal{F}_T(\omega)|^2, \text{ where } \mathcal{F}_T(\omega) = \int_0^T \widetilde{X}_n(t) e^{-i\omega t} dt$$

is the one-sided Fourier Transform, $\omega$ is the frequency and $i = \sqrt{-1}$. This PSD is related to the *autocovariance function*

$$\mathrm{R}_{X_n}(\tau) := \mathbb{E}\left[\widetilde{X}_n(t)\widetilde{X}_n(t+\tau)\right] = \lim_{T\to\infty} T^{-1} \int_0^T \widetilde{X}_n(t)\widetilde{X}_n(t+\tau) dt$$

by the well-known *Wiener-Khintchine Theorem* [50] that shows that the PSD can be expressed as the two-sided Fourier Transform of the autocovariance function

$$S_{X_n}(\omega) = \int_{-\infty}^{\infty} \mathrm{R}_{X_n}(\tau) e^{-i\omega\tau} d\tau. \tag{1.1}$$

The interpretation of the PSD curve is given below. The location $\omega_{\max}$ of its global maximum is considered to be the oscillatory frequency of the output signal.

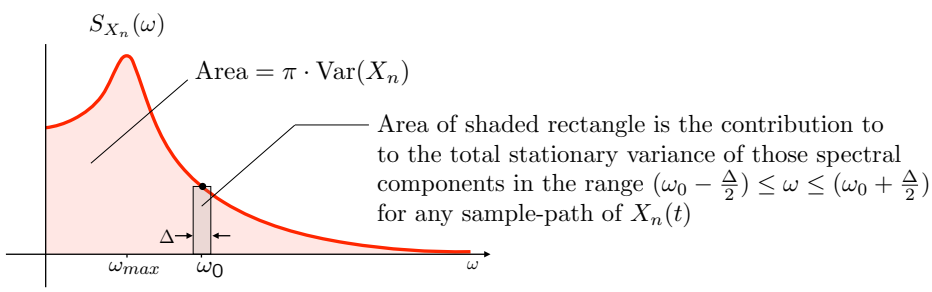


Commonly the PSD is estimated by first sampling a discrete time-series from a simulated CTMC trajectory at steady-state, and then taking its *Discrete Fourier Transform (DFT)* to estimate $\mathcal{F}_T(\omega)$ which then yields the PSD. This nonparametric procedure for PSD estimation is called the *periodogram* method and it has known drawbacks due to estimator bias and inconsistency that often manifests in a high variance of the PSD estimator. The reliability of the estimator can be improved by ensemble averaging, windowing or artificial smoothing [29], but the underlying problems that compromise the accuracy of the PSD estimate still remain.

information about the underlying network, and in order to access this information we need computational methods that can efficiently deduce the temporal correlation profile from a given stochastic reaction network model.

As is well-known in the engineering and physics communities among many others, frequency-domain analysis is a powerful way to analyse random signals and systematically study temporal correlations. In particular, a signal's *power spectral density (PSD)* measures the power content at each frequency, and it is related to the signal's temporal *autocovariance function* via the Fourier Transform (see Box 1). The PSD of a single-cell trajectory is intimately related to the underlying network's architecture and parametrisation *within the observed cell* [32] (see Figure 1 for an illustrative example). There exist a few studies that have successfully unravelled this relationship and discovered mechanistic principles for specific examples of reaction networks. For example, in [12] the role of feedback-induced delay in generating stochastic oscillations is explored and in [55] a stochastic amplification mechanism for oscillations is found. Other works in this direction have relied on approximating the CTMC with a *stochastic differential equation* (SDE) such as the Linear Noise Approximation (LNA) [74] or the chemical Langevin equation (CLE) [34]. With these SDE-based approaches the protein PSD for gene-regulatory networks was investigated in [68, 24, 69], the

relationship between input and output PSD for a single-input single-output system was computed in [71], and the single-cell PSD for a general bimolecular network in the vicinity of deterministic Hopf bifurcation was derived in [73]. Even though SDE approximations make the problem of computing the PSD analytically tractable, their accuracy is severely compromised if any of the species are in low copy-numbers [49], as is the case for many synthetic networks where low copy-numbers are desired in order to reduce metabolic load on the host cell [11]. Moreover, even when the species copy-numbers are uniformly large, the accuracy of SDE approximations can only be guaranteed over finite time-intervals [51], and hence the PSD, which is estimated at steady-state, may have a significant error. In order to address these issues, we need PSD computation methods that work reliably with CTMC models, and do not require any dynamical approximations. The aim of this paper is to develop such methods.

In a recent paper [70], the analytical relationship between the PSDs of the output species and its time-dependent production rate was derived for CTMC models of certain reaction networks including birth-death and simple gene-expression. While this analysis enables investigation of the dynamics of the protein creation process from experimentally measured protein time-traces, it does not extend to nonlinear networks, such as gene-expression networks with transcriptional feedback, for which some analytical results exist for simplified models [45].

A recurring theme in the existing literature is that typically the autocovariance function is well-approximated by the sum of a few exponential functions [70, 71, 24], and consequently the PSD is a rational function of a special form. This low dimensional feature can be theoretically explained by appealing to the compactness of the resolvent operator [47] associated with the CTMC, which we as prove, is connected to the PSD. Based on this connection we develop a Padé approximation [13] technique for estimating the PSD for a general stochastic reaction network, where the required Padé derivatives are estimated using a *single Monte Carlo trajectory simulation of the CTMC*. We design suitable covariates to improve the statistical precision of the derivative estimates and also provide a way to assess the accuracy of the Padé approximation. We refer to this PSD estimation method as *Padé PSD*.

Our approach is analytic in the case of linear networks, and we derive exact closed-form expressions for the PSD. For general nonlinear networks we take a *semi-analytic* approach, in the sense that the analytical expression for the PSD is found by first estimating certain quantities with simulation. Such approaches have become increasingly popular in recent years, as they provide viable solutions to nonlinear problems which are otherwise analytically intractable [20]. We show that in the special case of linear reaction networks, where all reaction propensity functions are affine functions of the state variables, we do not need to estimate any quantities via simulation, and the resolvent operator connection yields a purely analytical expression for the PSD. This result can be generalised to allow for arbitrary time-varying inputs and the resulting PSD has a special decomposition similar to what was found in previous SDE-based studies [71]. This result for linear networks also generalises the results in [70].

Given a stochastic reaction network model, commonly the single-cell PSD is estimated with nonparametric methods by first simulating a trajectory, and then sampling it at finitely-many timepoints to obtain a discrete time-series whose PSD can be straightforwardly computed with the Discrete Fourier Transform (DFT) [23]. Either one can apply the DFT directly to the time-series to estimate the PSD or one can first estimate the autocovariance function and then compute its DFT (see Box 1 for more details). While the latter approach is computationally very expensive due to autocovariance function computation, the former approach yields an inconsistent estimator for the PSD, which implies that the estimator variance does not vanish, even as the time-series length tends to infinity. To mitigate this inconsistency issue, PSDs from several independent trajectories are averaged, at the cost of significant computational burden as trajectory simulations are time-consuming. More importantly, the averaged PSD may still not be accurate because it is based on discrete sampling of continuous signals that can cause the problem of *aliasing* which distorts the estimated PSD by introducing frequency components corresponding to the sampling operation (see Chapter 1 in [29]). As shown by the Nyquist's Sampling Theorem [59] we can mitigate this aliasing effect by choosing the time-step parameter that is smaller than half of the reciprocal of the maximum frequency represented in the signal. However for stochastic dynamics it is difficult to use this criterion as the range of frequencies in the signal is very wide and picking a very small time-step can lead to computational intractability. These issues motivated us to devise a parametric approach to estimate the PSD that rather than relying on only the output signal, uses full information contained in the stochastic model of the dynamics. Our method does not require any discrete-sampling and it efficiently produces a reliable representation of the PSD with a computational cost

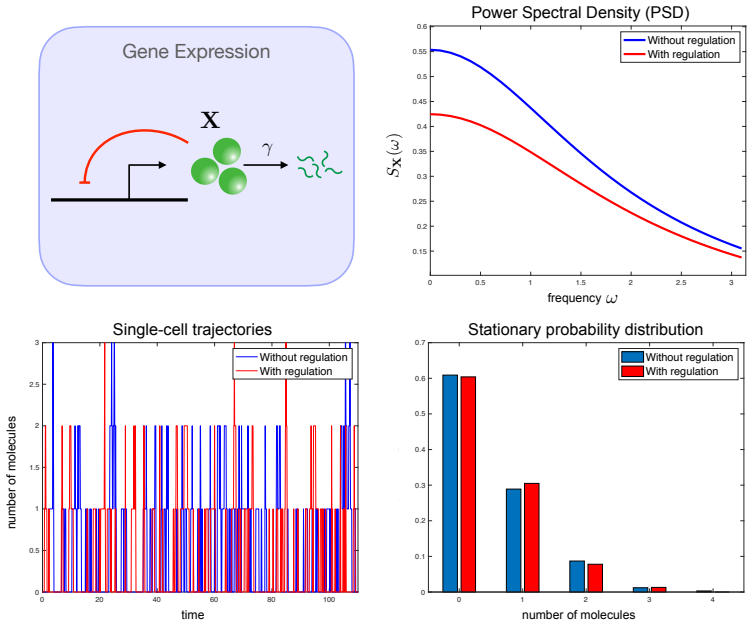


Figure 1: **The promise of frequency domain analysis.** We illustrate the potential of frequency domain analysis in understanding intracellular mechanisms with a toy example of a self-regulatory gene-expression system depicted above. This network consists of only one species $\mathbf{X}$ representing the protein output, which may repress its own expression as shown by the red arrow. The protein degrades at rate $\gamma$ and we model its expression rate via a Hill function as $(2-H)K^H/(K^H+x^H)$ where $H$ is the Hill coefficient, $K$ is some positive constant and $x$ is the copy-number of $\mathbf{X}$. Suppose we have two types of cells in a population, in the first there is no self-regulation (i.e. $H=0$) and so the production rate is constant at 1, and the second where there is active self-regulation with $H=1$. The steady-state single-cell trajectories appear to be similar for both cell-types (see the *bottom-left* figure above) and hence differentiating between them is difficult in the time-domain. Even the stationary probability distribution for both subpopulations is almost identical (see the *bottom-right* figure above) and hence flow cytometry measurements cannot distinguish among the cell-types. However, frequency domain analysis of the temporal fluctuations at steady-state can indeed differentiate the cell-types as demonstrated by distinctive PSDs (see the *top-right* figure above). This highlights the importance of exploiting time correlations of single-cell trajectories (and their frequency domain representations) in understanding intracellular reaction mechanisms. The PSDs in this example are estimated by the Padé PSD method developed in this paper.

which is comparable to nonparametric methods.

We illustrate our results with applications of relevance to both systems and synthetic biology. Using the analytic theory we develop for linear networks, we demonstrate how PSDs enable differentiation between two fundamental types of adapting circuit topologies, viz. Incoherent Feedforward (IFF) and Negative Feedback (NFB) [53], in the presence of dynamical intrinsic noise. We also examine how PSD estimation can help in examining the phenomenon of single-cell entrainment in the stochastic setting. Employing the Padé approximation theory for estimating the PSDs of general nonlinear networks we illustrate how the performance of certain synthetic circuits, with noisy dynamics, can be optimised. Specifically we examine the problem of optimising the oscillation strength of a well-known synthetic oscillator (called the *repressilator* [28]) and the problem of reducing oscillations at the single-cell level which can arise when an intracellular network is controlled with the recently proposed *antithetic integral feedback* (AIF) controller [14] that has the important property of ensuring robust perfect adaptation despite randomness in the dynamics and other environmental uncertainties.

# 2 The resolvent representation of the PSD

In this section, we describe the CTMC model for a reaction network and define the resolvent operator associated with it. We then connect this operator to the PSD. This connection shall be exploited in later sections to develop our analytical and computational PSD results.

## 2.1 The Stochastic Model

Consider a reaction network with $d$ species, called $\mathbf{X}_1, \ldots, \mathbf{X}_d$, and $K$ reactions. In the classical stochastic reaction network model, the dynamics is described as a *continuous-time Markov chain* (CTMC) [2] whose states represent the copy numbers of the $d$ network species. If the state is $x = (x_1, \ldots, x_d)$ and reaction $k$ fires, then the state is displaced by the integer stoichiometric vector $\zeta_k$. The rate of firing for reaction $k$ at state $x$ is governed by the propensity function $\lambda_k(x)$. Under the mass-action hypothesis [2]

$$\lambda_k(x_1, \ldots, x_d) = \theta_k \prod_{j=1}^{d} \frac{x_j(x_j - 1)\ldots(x_j - \nu_{jk} + 1)}{\nu_{jk}!}, \tag{2.2}$$

where $\theta_k$ is the rate constant and $\nu_{jk}$ is the number of molecules of $\mathbf{X}_j$ consumed by the $k$-th reaction. Formally, the CTMC $(X(t))_{t\geq 0}$ representing the reaction kinetics can be defined by its generator $\mathbb{A}$, which is an operator that specifies the rate of change of the probability distribution of the process (see Chapter 4 in [30]). It is defined by

$$\mathbb{A}f(x) = \sum_{k=1}^{K} \lambda_k(x) \left( f(x + \zeta_k) - f(x) \right), \tag{2.3}$$

for any real-valued bounded function $f$ on the state-space which consists of all accessible states in the $d$-dimensional non-negative integer lattice.

For each state $x$, let $p(t, x)$ be the probability that the CTMC $(X(t))_{t\geq 0}$ is in state $x$ at time $t$. Then these probabilities evolve according to a system of ordinary differential equations, called the Chemical Master Equation (CME) [2], which is typically unsolvable. Hence its solutions are often estimated with Monte Carlo simulations of the CTMC, using methods such as Gillespie's *stochastic simulation algorithm* (SSA) [33]. If the CME has a unique, globally attracting fixed point $\pi$ then the CTMC is called *ergodic* with $\pi$ as the stationary distribution. If the convergence of $p(t)$ to $\pi$ is exponentially fast in $t$, then the CTMC is called exponentially ergodic and the exponential rate of convergence is called the *mixing strength* of the CTMC. We shall work under the assumption of exponential ergodicity which is computationally verifiable using techniques in [37] and [38], wherein, it is also demonstrated that this assumption is satisfied for networks typically encountered in systems and synthetic biology. It is very important to note that for an ergodic network, all stochastic trajectories, despite being different, have the same PSD.

## 2.2 The Resolvent Operator and its connection to the PSD

The resolvent operator corresponding to the generator $\mathbb{A}$ of the CTMC $(X(t))_{t\geq 0}$ plays a central role in the development of our method for PSD estimation. For any complex number $s$ and a given function $f(\cdot)$ on the state space, the resolvent operator can be defined as

$$\mathbb{R}(s)f(x) = (s\mathbf{I} - \mathbb{A})^{-1} f(x) = \sum_{k=0}^{\infty} s^{-(k+1)} \mathbb{A}^k f(x), \tag{2.4}$$

where $\mathbf{I}$ is the identity operator. Conditioned on the event that the CTMC $(X(t))_{t\geq 0}$ starts at initial state $X(0) = x$, $\mathbb{R}(s)f(x)$ is essentially the Laplace Transform of the signal given by the expected value of the random variable $f(X(t))$, i.e.

$$\mathbb{R}(s)f(x) = \int_0^{\infty} e^{-st} \mathbb{E}\left(f(X(t))|X(0) = x\right) dt.$$

Assuming that the observed single-cell trajectory $(X_n(t))_{t\geq 0}$ is the copy-number dynamics of output species $\mathbf{X}_n$, we now establish a relation between the PSD $S_{X_n}(\omega)$ (see Box 1) and the resolvent operator. Let $\mathbb{E}_\pi(X_n)$ denote the stationary expectation of the copy-number of species $\mathbf{X}_n$ and let $f$ be the function

$$f(x) = x_n - \mathbb{E}_\pi(X_n). \tag{2.5}$$

Defining $G(s) := \mathbb{E}_\pi\left(f\mathbb{R}(s)f\right)$, the PSD $S_{X_n}(\omega)$ is given by

$$S_{X_n}(\omega) = 2\text{Real}(G(i\omega)), \tag{2.6}$$

where $i = \sqrt{-1}$. This relation is proved in Section S2.2 of the Supplement. In this result we view the function $x \mapsto f(x)\mathbb{R}(s)f(x)$ as a random variable on the probability space whose sample-space is the state-space of the CTMC and the probability distribution given by the stationary distribution $\pi$. The expectation of this random variable is denoted by $G(s)$ and in the PSD estimation method we develop, we first estimate $G(s)$ and then obtain the PSD using (2.6).

In the case of linear networks, $G(s)$ can be exactly computed and this yields an analytical formula for the PSD which is presented in the next section. For general nonlinear networks, we base our PSD estimation on the eigen-decomposition of the resolvent operator which allows us to express $G(s)$ as an infinite sum

$$G(s) = \sum_{j=1}^{\infty} \frac{\alpha_j}{s - \sigma_j}, \tag{2.7}$$

where $\sigma_1, \sigma_2, \ldots$ are the non-zero eigenvalues of $\mathbb{A}$, arranged in descending order of their real parts (which are negative due to ergodicity). Each coefficient $\alpha_j$ captures the power in the signal corresponding to eigenmode $\sigma_j$, and their sum is equal to the total signal power which is also the stationary variance $\text{Var}_\pi(X_n)$ of the output species copy-number

$$\sum_{j=1}^{\infty} \alpha_j = \text{Var}_\pi(X_n).$$

Relation (2.7) is equivalent to the following representation of the autocovariance function

$$\text{R}_{X_n}(\tau) = \sum_{j=1}^{\infty} \alpha_j e^{\sigma_j \tau}. \tag{2.8}$$

# 3 Spectral theory for linear networks

In this section we consider linear networks where all reaction propensity functions are affine functions of the state variables. Under mass-action kinetics, linear networks are necessarily unimolecular, i.e. all reactions

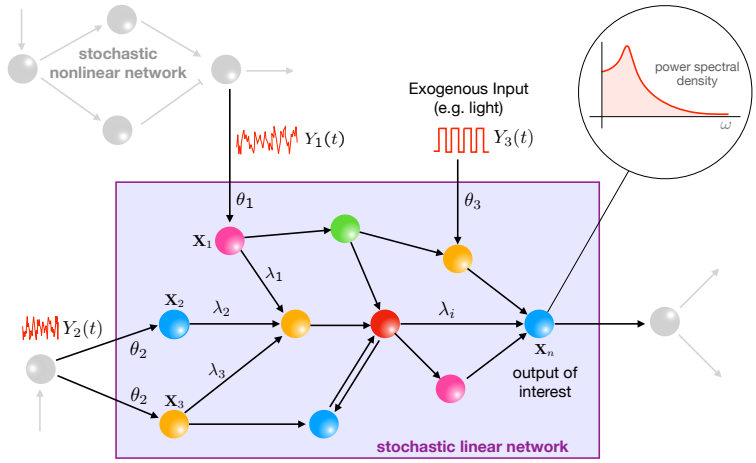


Figure 2: **The setting of the PSD decomposition result:** A stochastic reaction network with linear propensity functions embedded in the intracellular milieu and receiving stimulation from several upstream networks. Theorem 3.2 provides an analytical decomposition for the output PSD $S_{X_n}(\omega)$ in terms of the PSDs of all the stimulating signals.

have at most one reactant and are of the form $\emptyset \longrightarrow \star$ or $\mathbf{X_i} \longrightarrow \star$, where $\star$ represents any linear combination of species. Assuming $d$ species and $K$ reactions, for linear networks we can express the vector of propensity functions $\lambda(x) = (\lambda_1(x), \ldots, \lambda_K(x))$ as an affine map on the state-space

$$\lambda(x) = \Lambda x + \widetilde{b},$$

where $\Lambda$ is some $K \times d$ matrix and $\widetilde{b}$ is a $K \times 1$ vector. Letting $S$ be the $d \times K$ matrix whose columns are the stoichiometric vectors $\zeta_1, \ldots, \zeta_K$ for the reactions. We define

$$A = S\Lambda \qquad \text{and} \qquad b = S\widetilde{b},$$

and under the assumption of ergodicity, the $d \times d$ matrix $A$ is Hurwitz-stable, i.e. all its eigenvalues have strictly negative real parts. It can be easily shown (see [37] for e.g.) that the dynamics of the expected state $x(t) = \mathbb{E}(X(t))$ is given by

$$\frac{dx}{dt} = Ax(t), \tag{3.9}$$

and as $t \to \infty$, $x(t)$ converges to $\overline{x}$ which is the state expectation under the stationary distribution $\pi$

$$\overline{x} = \mathbb{E}_\pi(X) = -A^{-1}b.$$

Moreover the stationary covariance matrix $\Sigma$ for the state can be computed by solving the following Lyapunov equation

$$A\Sigma + \Sigma A^T + DD^T = 0,$$

where $D$ is the positive semidefinite matrix satisfying $DD^T = S\text{diag}(\Lambda\overline{x} + \widetilde{b})S^T$. In this setting, we can show that the resolvent operator maps the class of affine functions to itself, and this allows us to apply expression (2.6) to prove (see the Supplement, Section S2.3) the following:

**Theorem 3.1 (PSD Analytic Expression)** *Let $e_n$ denote the $n$-th column of the $d \times d$ identity matrix $\mathbf{I}$. Then*

$$S_{X_n}(\omega) = -2e_n^T(\omega^2\mathbf{I} + A^2)^{-1}A\Sigma e_n.$$

This result gives a simple explicit formula for computing the PSD of the dynamics of the output species $\mathbf{X}_n$ for linear networks.

### Connections with Linear ODEs Driven by Gaussian Noise

We now relate this result with a familiar result in theory of Gaussian processes. Consider the SDE obtained by perturbing the deterministic linear system (3.9) by $d$-dimensional white noise $\xi(t)$ as follows

$$\frac{dx}{dt} = Ax(t) + D\xi(t). \tag{3.10}$$

This is a multivariate Ornstein-Uhlenbeck process with zero steady-state mean vector and $\Sigma$ as the steady-state variance-covariance matrix. As shown in [65], the autocovariance function for this process is given by

$$\mathrm{R}_{x_n}(\tau) = e_n^T e^{A\tau} \Sigma e_n$$

and applying the Wiener-Khintchine Theorem (see Box 1) we obtain the PSD by computing the Fourier Transform of $\mathrm{R}_{x_n}(\tau)$ as

$$S_{x_n}(\omega) = 2\mathrm{Real}(e_n^T (i\omega - A)^{-1} \Sigma e_n)$$

which is identical to the PSD expression given in Theorem 3.1. Hence for linear reaction networks, the exact PSD can be derived by approximating the CTMC with the SDE (3.10), which can be viewed as the Linear Noise Approximation (LNA) of the CTMC dynamics.

## 3.1 Linear reaction networks stimulated by external inputs

We now generalise our PSD analysis for linear networks by considering the situation where such a network is being driven by external signals. These signals could be generated by different sources, e.g. upstream interconnected networks, environmental stimuli, or by engineered inputs introduced to probe the dynamics (see Figure 2). A fundamentally important question is to understand how the internal noise and each of these inputs (deterministic or stochastic) conspire to make up the full power spectrum of an output of interest. Indeed it would be of considerable conceptual and practical significance to be able to decompose the output power spectrum in a way that allows the quantification of the specific contributions to the spectrum of the internal noise and of each of the external inputs. Although approximate decompositions of this sort have been reported in specific simple example networks modeled by CLEs [71, 69], to the best of our knowledge no spectral decomposition results exist for general biochemical networks modeled by CLE, nor for those modeled by discrete-stochastic CTMC models.

We consider $m$ independent time-varying signals $(Y_1(t))_{t\geq 0}, \ldots, (Y_m(t))_{t\geq 0}$. We assume that these signals stimulate through $m$ zeroth-order reactions of the form

$$\emptyset \xrightarrow{\theta_k Y_k(t)} \sum_{j=1}^{d} c_{jk} \mathbf{X_j} \tag{3.11}$$

for $k = 1, \ldots, m$. Each reaction follows mass-action kinetics and for reaction $k$, $\theta_k$ is a positive constant and $c_k = (c_{1k}, \ldots, c_{dk})$ is the vector representing the number of molecules of each species $\mathbf{X_1}, \ldots, \mathbf{X_d}$ created by this reaction. We shall assume that process $(Y(t))_{t\geq 0}$, which includes all the stimulating signals, is an exponentially ergodic Markov process with stationary expectation $\overline{y} = (\overline{y}_1, \ldots, \overline{y}_m)$. Let $\overline{\Sigma}$ be the stationary variance-covariance matrix for the process $(X(t))_{t\geq 0}$ *when each stimulating signal is deterministic and fixed to its stationary mean at all times*, i.e. $Y(t) = \overline{y}$ for all $t \geq 0$. We now present our main result for linear networks which provides an analytic relationship between the PSD $S_{X_n}(\omega)$ of our output species $\mathbf{X_n}$ and the of PSDs $S_{Y_j}(\omega)$ for $j = 1, \ldots, m$.

**Theorem 3.2 (PSD Decomposition)** *Consider a unimolecular reaction network comprising species* $\mathbf{X_1}, \ldots, \mathbf{X_d}$, *stimulated by independent time-varying signals* $(Y_1(t))_{t\geq 0}, \ldots, (Y_m(t))_{t\geq 0}$, *through zeroth-order reactions of the form* (3.11). *We assume that each* $Y_j$ *is an exponentially ergodic Markov process with PSD* $S_{Y_j}(\omega)$. *The*

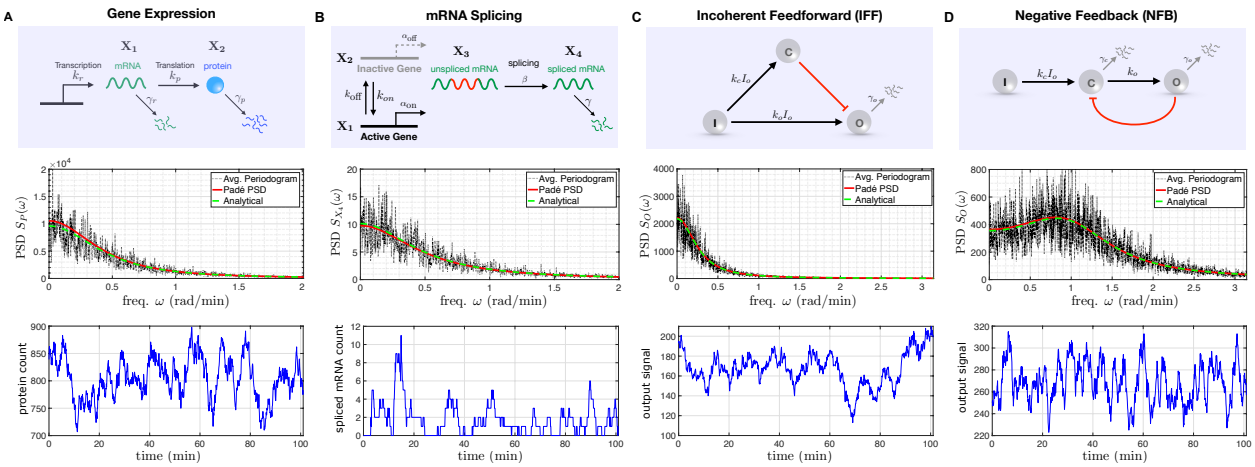


Figure 3: **Frequency domain analysis of linear propensity networks:** (A) This is the standard gene-expression model where mRNA ($\mathbf{X_1}$) is transcribed constitutively and it translates into protein ($\mathbf{X_2}$). (B) In this RNA splicing network a gene can randomly switch between inactive ($\mathbf{X_1}$) (low transcription) and active ($\mathbf{X_2}$) (high transcription) states. When transcription occurs, unspliced mRNA ($\mathbf{X_3}$) is created which is then converted into spliced mRNA ($\mathbf{X_4}$) by the splicing machinery. (C) In the Incoherent Feedforward (IFF) network an input $\mathbf{I}$ (constant level $I_0$) directly produces the output $\mathbf{O}$ and it produces a controller species $\mathbf{C}$, which represses the production of output $\mathbf{O}$. (D) In the Negative Feedback (NFB) network the input $\mathbf{I}$ (constant level $I_0$) produces the controller species $\mathbf{C}$, that produces the output species $\mathbf{O}$ which in turn inhibits the production of $\mathbf{C}$ from $\mathbf{I}$. For all the networks single-cell output trajectories in the stationary phase are plotted. We provide a comparison of the single-cell PSDs estimated with three approaches - 1) analytically with expressions (3.13), (3.15), (3.17) and (3.22), 2) the Padé PSD method described in Section 4 (using one simulated trajectory) and 3) the averaged periodogram method mentioned in Box 1 (using discrete samples from ten simulated trajectories). For the NFB network one can see that detecting the presence of oscillations in the fluctuations is much easier in the frequency-domain than in the time-domain. We indicate the location $\omega_{\max}$ of the PSD maxima which is computed using expression (4.30).

*PSD of the output species* $\mathbf{X_n}$ *is given by*

$$S_{X_n}(\omega) = \underbrace{-2e_n^T(\omega^2\mathbf{I} + A^2)^{-1}A\overline{\Sigma}}_{\text{intrinsic}} + \underbrace{\sum_{j=1}^{m} \theta_j^2 |e_n^T(A + i\omega\mathbf{I})^{-1}c_j|^2 S_{Y_j}(\omega)}_{\text{extrinsic}}.$$

The proof of this result is provided in Section S2.3 in the Supplement and it shows that the output spectrum is the sum of the intrinsic contribution and the external contributions from all stimulating signals. The external contribution due to signal $Y_j$ is modulated by the frequency dependent gain $\theta_j^2|e_n^T(A + i\omega\mathbf{I})^{-1}c_j|^2$.

## 3.2 Applications of the linear theory

We now present various applications of the results developed in this section. We start by providing analytical expressions for the PSD of certain simple networks, like the birth-death, the classical gene-expression network [72] and the recently proposed RNA splicing network [9]. Next we discuss how our results on PSD estimation can enable us to differentiate between adapting circuit topologies [53] and lastly we examine how the PSD decomposition result (Theorem 3.2) can help us in studying the phenomenon of single-cell entrainment in the stochastic setting. Detailed descriptions of the networks considered in the paper and their PSD analysis can be found in Section S4 of the Supplement. All propensity functions are assumed to follow mass-action kinetics (2.2) unless stated otherwise.

### 3.2.1 Gene Transcription

Consider a simple model of constitutive gene transcription and mRNA degradation consisting of a single-species birth-death network with rate of production $k$ and the rate of degradation $\gamma$

$$\emptyset \xrightarrow{k} \mathbf{X} \xrightarrow{\gamma} \emptyset.$$

The stationary distribution for this network is Poisson with parameter $k/\gamma$. Hence the stationary mean and variance and equal to $k/\gamma$ and applying Theorem 3.1 we can compute the PSD as

$$S_X(\omega) = \frac{2k}{\gamma^2 + \omega^2}. \tag{3.12}$$

This shows that up to a multiplicative constant, the PSD follows the fat-tailed *Cauchy Distribution* with infinite mean and variance. Observe that if the timescale of the process is changed (i.e. both $k$ and $\gamma$ are multiplied by a positive constant), then the stationary distribution remains invariant but the PSD will get altered. This shows that for parameter inference problems, the PSD of single-cell trajectories carries more information than population-level measurements provided by Flow-Cytometry.

### 3.2.2 Gene Expression Network

We now analyse the gene-expression model shown in Figure 3(A) that consists of two species - the mRNA ($\mathbf{X_1}$) and the protein ($\mathbf{X_2}$). There are four reactions corresponding to mRNA transcription, protein translation and the first-order degradation of both the species. Observe that the mRNA dynamics is birth-death and hence we can compute its PSD using (3.12) with $(k, \gamma) \mapsto (k_r, \gamma_r)$. Since mRNA stimulates the creation of protein via a reaction of the form (3.11) we can apply our PSD Decomposition result (Theorem 3.2) to express the protein PSD as a sum of two components corresponding to translation and transcription respectively:

$$S_{X_2}(\omega) = \underbrace{\frac{2k_r k_p}{\gamma_r(\gamma_p^2 + \omega^2)}}_{\text{translation}} + \underbrace{\frac{k_p^2}{\gamma_p^2 + \omega^2}\frac{2k_r}{\gamma_r^2 + \omega^2}}_{\text{transcription}}. \tag{3.13}$$

The translation term is computed by setting the mRNA level to its stationary mean $\overline{x}_1 := k_r/\gamma_r$ and then viewing the protein dynamics as a birth-death process with production rate $k_p x_1$ and degradation rate $\gamma_p$. The transcription term is simply the PSD of mRNA modulated by the frequency dependent factor given by Theorem 3.2.

### 3.2.3 RNA Splicing network

The recently proposed RNA Splicing network (see Figure 3(B)) was used to model the concept of RNA velocity that can help in understanding cellular differentiation from single-cell RNA-sequencing data [9]. Here a single gene-transcript can randomly switch between inactive ($\mathbf{X_1}$) and active ($\mathbf{X_2}$) states with different rates of transcription of unspliced mRNA ($\mathbf{X_3}$). The splicing process converts these unspliced mRNAs into spliced mRNAs ($\mathbf{X_4}$) that can then undergo first-order degradation. Applying Theorem 3.1 we can write the PSD of the dynamics of active gene count as

$$S_{X_2}(\omega) = \frac{2k_{\text{on}}k_{\text{off}}}{(k_{\text{on}} + k_{\text{off}})(k_{\text{on}} + k_{\text{off}} + \omega^2)}. \tag{3.14}$$

Note that when the active gene count is $X_2 \in \{0, 1\}$ the transcription rate is $\alpha_{\text{off}} + (\alpha_{\text{on}} - \alpha_{\text{off}})X_2$. We can view transcription as a superposition of two reactions - a constitutive reaction with rate $\alpha_{\text{off}}$ and reaction of the form (3.11) where the stimulant is the active gene $\mathbf{X_2}$. Applying Theorem 3.2 we can decompose the PSD of the spliced mRNA count as

$$S_{X_4}(\omega) = \underbrace{\frac{2(\alpha_{\text{off}}k_{\text{off}} + \alpha_{\text{on}}k_{\text{on}})}{(k_{\text{off}} + k_{\text{on}})(\gamma^2 + \omega^2)}}_{\text{splicing}} + \underbrace{\frac{\beta^2(\alpha_{\text{on}} - \alpha_{\text{off}})^2}{(\beta^2 + \omega^2)(\gamma^2 + \omega^2)}S_{X_2}(\omega)}_{\text{transcription}}, \tag{3.15}$$

where $S_{X_2}(\omega)$ is given by (3.14).

### 3.2.4 Differentiation between adapting regulatory topologies

We consider the simple three-node IFF and NFB topologies depicted in Figure 3(C,D) with stochastic kinetics. We provide analytical expressions for the PSD under the assumption of linearised propensity functions for the repression mechanisms. These expressions inform us about qualitative *structural* differences between the PSDs obtained from IFF and NFB topologies, regardless of the choice of reaction rate parameters. This shows that in the stochastic setting, the PSD of single-cell trajectories serves as a key "response signature" that can differentiate between adapting circuit topologies.

We begin by analysing the IFF topology, where the controller species **C** catalytically produces the output species **O** at rate $F_f(x_c)$ which is a monotonically decreasing function of the controller species copy-number $x_c$ and it represents the repression of **O** by **C**. We linearise the function $F_f(x_c)$ as

$$F_f(x_c) = \beta_0 - \beta_{\text{ff}} x_c, \tag{3.16}$$

where $\beta_0$ and $\beta_{\text{ff}}$ are positive constants denoting the *basal* production rate and the strength of the incoherent feedforward mechanism respectively. With this linearisation, all propensity functions become affine and hence we can apply the results from Section 3 for unimolecular networks. Specifically the steady-state means $\overline{x}_c := \mathbb{E}_\pi(C)$ and $\overline{x}_o := \mathbb{E}_\pi(O)$ are given by

$$\overline{x}_c = \frac{k_c I_0}{\gamma_c} \quad \text{and} \quad \overline{x}_o = \frac{k_o I_0 + \beta_0}{\gamma_o} - \frac{\beta_{\text{ff}} k_c I_0}{\gamma_c \gamma_o}$$

and it is immediate that if $\beta_{\text{ff}} \approx k_o \gamma_c / k_c$, then the mean output value $\overline{x}_o \approx \beta_0/\gamma_o$ becomes insensitive to the input abundance level $I_0$. This shows the adaptation property of the IFF network. Applying Theorem 3.1 we obtain the following expression for the PSD for the output trajectory

$$S_O(\omega) = \frac{2}{\gamma_o^2 + \omega^2} \left[ \beta_0 + k_o I_0 - \frac{\beta_{\text{ff}} k_c I_0}{\gamma_c} + \frac{\beta_{\text{ff}}^2 k_c I_0}{\gamma_c^2 + \omega^2} \right]. \tag{3.17}$$

This form of the PSD function allows us to conclude that output trajectories cannot show oscillations, as the mapping $\omega \mapsto S_O(\omega)$ is monotonically decreasing *regardless of the IFF network parameters.*

In the NFB topology, the production of the controller species **C** is repressed by the output species **O**, and we model the production rate by a monotonically decreasing function $F_b(x_o)$ of the output species copy-number $x_o$. As before, we linearise this function as

$$F_b(x_o) = \beta_0 - \beta_{\text{fb}} x_o, \tag{3.18}$$

where $\beta_0$ is the basal production rate and $\beta_{\text{fb}}$ is the feedback strength. Under this linearisation, the steady-state means $\overline{x}_c := \mathbb{E}_\pi(C)$ and $\overline{x}_o := \mathbb{E}_\pi(O)$ are given by

$$\overline{x}_c = \frac{\gamma_o \beta_0 I_0}{\gamma_c \gamma_o + k_o \beta_{\text{fb}} I_0} \quad \text{and} \quad \overline{x}_o = \frac{k_o \beta_0 I_0}{\gamma_c \gamma_o + k_o \beta_{\text{fb}} I_0}.$$

Observe that if the input abundance level $I_0$ is high, then mean output value $\overline{x}_o \approx \beta_0/\beta_{\text{fb}}$ only depends on the feedback function $F_b$ and it is insensitive to $I_0$, thereby demonstrating the adaptation property. Applying Theorem 3.1 we arrive at the following expression for the PSD for the output trajectory

$$\begin{aligned} S_O(\omega) = &\frac{2\gamma_o k_o \beta_0 I_0}{\gamma_c \gamma_o + k_o \beta_{\text{fb}} I_0} \\ &\times \left[ \frac{\gamma_c^2 + k_o \gamma_c + \omega^2}{(\gamma_c \gamma_o + k_o \beta_{\text{fb}} I_0)^2 + \omega^2 (\gamma_c^2 + \gamma_o^2 - 2 k_o \beta_{\text{fb}} I_0) + \omega^4} \right]. \end{aligned} \tag{3.19}$$

Simple analysis reveals that the mapping $\omega \mapsto S_O(\omega)$ has a positive local maximum (which is also the global maximum) if and only if

$$k_o \beta_{\text{fb}} I_0 > \frac{\gamma_c^4 + \gamma_c^3 k_o + \gamma_o^2 \gamma_c k_o}{\sqrt{\Gamma(\gamma_c, \gamma_o, k_o)} + \gamma_c \gamma_o + \gamma_c^2 + k_o \gamma_c}, \tag{3.20}$$

where $\Gamma(\gamma_c, \gamma_o, k_o) := (\gamma_c\gamma_o + \gamma_c^2 + k_o\gamma_c)^2 + \gamma_c^4 + \gamma_c^3 k_o + \gamma_o^2\gamma_c k_o$. This condition shows that *regardless of the choice of NFB network parameters*, the output trajectories will exhibit oscillation if the input abundance level $I_0$ is high enough. This differentiates it from the IFF circuit which never exhibits oscillations. Note that high $I_0$ is precisely the condition for NFB to show adaptation and hence imposing this requirement is not very restrictive. The role of negative feedback is causing stable stochastic oscillations was explored theoretically in [45] with CLE, and it has also been demonstrated experimentally. This PSD-based criterion for differentiating between adapting IFF and NFB topologies can be extended beyond three-node motifs to allow for an arbitrary number of nodes (see the Supplement, Section S4.1.3).

For a specific parameterisation of the gene-expression, the RNA splicing, the IFF and the NFB networks, we compare the PSDs obtained analytically with those obtained by our Padé PSD method described in Section 4 and the averaged periodogram approach (see Box 1). The results are presented in Figure 3 and they show good agreement, despite the noisy nature of the periodogram estimate. Since negative propensities cannot be allowed, we perform simulations with the positive part of the linear feedforward (see (3.16)) and feedback (see (3.18)) functions. Hence the analytical PSD expressions for the IFF and the NFB networks are not exact.

### 3.2.5 Stochastic entrainment by a noisy upstream oscillator

The phenomenon of entrainment occurs when an oscillator, upon stimulation by a periodic input, loses its natural frequency and adopts the frequency of the input. This phenomenon has several applications in physical, engineering and biological systems [61]. The most well-known biological example of this phenomenon is the entrainment of the circadian clock oscillator by day-night cycles. The circadian clock is an organism's time-keeping device and its entrainment is necessary to robustly maintain its periodic rhythm [7]. The circadian clock is one example among several intracellular oscillators that have been found and their functional roles have been identified [10]. Often these oscillators provide entrainment cues to other networks within cells [63] and hence it is important to study entrainment at the single-cell level, where the dynamics is intrinsically noisy due to low copy-number effects.

We now illustrate how the results in this paper can be used to study single-cell entrainment in the stochastic setting where the dynamics is described by CTMCs. We consider the example of the *repressilator* stimulating a gene-expression system, as shown in Figure 4(A). This gene-expression network is the same as in Section 3.2.2, but we include transcriptional feedback from the protein molecules and so the mRNA transcription rate is given by a monotonic decreasing function $F_b(x_2)$ of the protein copy-number $x_2$. We shall linearize $F_b(x_2)$ as

$$F_b(x_2) = k_r - k_{\text{fb}} x_2,$$

where $k_r$ is the basal transcription rate and $k_{\text{fb}}$ is the feedback strength. When this gene-expression network is connected to the *repressilator* (described later in Section 4.1.1) the transcription rate changes from $F_b(x_2)$ to

$$\theta p_2 + F_b(x_2), \tag{3.21}$$

where $p_2$ is the molecular count of protein cI in the *repressilator* and parameter $\theta$ captures the "strength" of the interconnection. In other words, cI acts as an activating transcription factor in our example. The parameters of the *repressilator* are chosen as in Section 4.1.1 in the "no sponge" and Hill coefficient $H = 1.5$ case, but the time-units are changed to minutes. We can view the gene-expression network as simply the negative feedback (NFB) network from Section 3.2.4 with the controller species $\mathbf{C}$ as mRNA $\mathbf{X_1}$ and the output species $\mathbf{O}$ as protein $\mathbf{X_2}$. Using the same parameters as the NFB network, we study how the PSD of the protein output varies as a function of $\theta$. In order for the gene-expression network to be entrained to the *repressilator* the global maxima of this protein PSD should be near the *repressilator's* natural (or peak) frequency of about 1.37 rad./min (see Figure 4(B)).

To compute the PSD of the combined network we shall apply Theorem 3.2. For this we first consider the gene-expression network in isolation with $p_2$ in the transcription rate (3.21) replaced by the constant steady-state mean of $p_2$ (denoted by $\mathbb{E}_\pi(P_2)$). Hence using (3.19) we can estimate the protein dynamics PSD

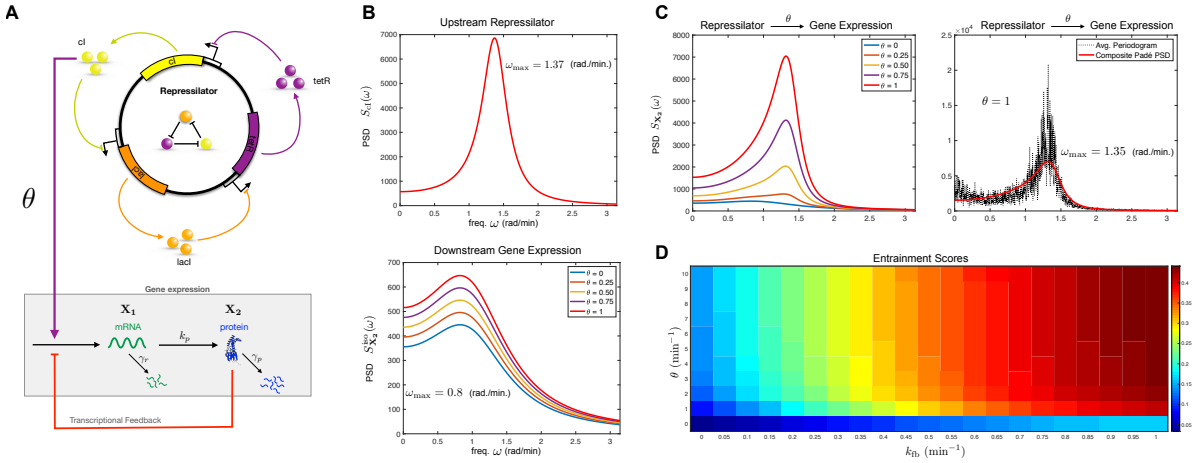


Figure 4: **Stochastic entrainment of gene-expression by the *repressilator*:** (A) Schematic diagram of the *repressilator* driving a gene-expression network. The cI protein from the *repressilator* acts as an activating transcription factor for mRNA ($\mathbf{X_1}$) which translates into output protein ($\mathbf{X_2}$). The red arrow from $\mathbf{X_2}$ to $\mathbf{X_1}$ indicates negative transcriptional feedback from the protein molecules. (B) The PSDs for the upstream *repressilator* network (estimated with Padé PSD; see Figure 5(B)) and the downstream gene-expression network in isolation (i.e. not connected to the *repressilator*) for five values of the connection strength parameter $\theta$ (in $\text{min}^{-1}$). The gene-expression PSDs are computed analytically (see (3.19)). When the *repressilator* is connected to the gene-expression expression, the PSD can be estimated with the *composite* Padé PSD method which is based on Theorem 3.2. In (C) these PSD estimates are plotted five values of $\theta$ and compared for $\theta = 1$ $\text{min}^{-1}$ to the PSDs obtained with the averaged periodogram approach. One can observe *stochastic entrainment* improves as $\theta$ gets larger. (D) The heat-map for the entrainment score (see (3.23)) as a function of $\theta$ and the feedback strength parameter $k_{\text{fb}}$. Observe that the entrainment score is monotonically increasing in both variables but it is more sensitive to $k_{\text{fb}}$ than $\theta$.

$S^{\text{iso}}_{X_2}(\omega)$ as

$$S^{\text{iso}}_{X_2}(\omega) = \frac{2\gamma_p k_p(\theta \mathbb{E}_\pi(P_2) + k_r)}{\gamma_r\gamma_p + k_p k_{\text{fb}}} \times \left[\frac{\gamma_r^2 + k_p\gamma_r + \omega^2}{(\gamma_r\gamma_p + k_p k_{\text{fb}})^2 + \omega^2(\gamma_r^2 + \gamma_p^2 - 2k_p k_{\text{fb}}) + \omega^4}\right].$$

It is immediate that irrespective of the value of $\theta$, the PSD $S^{\text{iso}}_{X_2}(\omega)$ has a global maxima at $\omega_{\max} \approx 0.8$ rad./min. which is the natural frequency of the gene-expression circuit in isolation. In Figure 4(B) we plot this PSD for five values of $\theta$ to illustrate this point.

When the *repressilator* is connected to the gene-expression network, we can apply Theorem 3.2 to compute the PSD of the protein output as

$$S_{X_2}(\omega) = S^{\text{iso}}_{X_2}(\omega) + \left[\frac{\theta^2 k_p^2}{(\gamma_r\gamma_p + k_p k_{\text{fb}})^2 + \omega^2(\gamma_r^2 + \gamma_p^2 - 2k_p k_{\text{fb}}) + \omega^4}\right] S_{cI}(\omega). \tag{3.22}$$

We call this method *composite* Padé PSD as it estimates the PSD for the full network by combining two approaches - Padé PSD for the nonlinear subnetwork (*repressilator*) with the analytical expression for the linear subnetwork (gene-expression). In Figure 4(C) we plot the PSD $S_{X_2}(\omega)$ for five values of $\theta$ and we validate this composite method with the averaged periodogram method. One can clearly see that as $\theta$ gets higher, the gene-expression network gives up its natural frequency ($\approx 0.8$ rad./min) upon stimulation and adopts a frequency which is close to the *repressilator* frequency. This exemplifies the phenomenon of single-cell entrainment in the stochastic setting.

In order to investigate this entrainment phenomenon further we define an *entrainment score* as

$$\text{Entrainment Score} = \frac{\int_{\omega_l}^{\omega_r} S_{X_2}(\omega)d\omega}{\int_0^\infty S_{X_2}(\omega)d\omega}, \tag{3.23}$$

where $[\omega_l, \omega_r] = [0.9\omega_0, 1.1\omega_0]$ represents an interval of relative length 10% on either side of the *repressilator's* natural frequency $\omega_0$. In Figure 4(D) we plot a heat-map for the entrainment score as a function of the feedback strength parameter $k_{\text{fb}}$ and the connection strength parameter $\theta$. One can see that the entrainment score increases monotonically with $\theta$ which is to be expected as the first term on the r.h.s. of (3.22) scales linearly with $\theta$ while the second term scales quadratically. Similarly by computing the ratio of the two terms we can conclude that entrainment score is also a monotonically increasing function of $k_{\text{fb}}$. However as the heat-map clearly indicates, the entrainment score is much more sensitive to $k_{\text{fb}}$ than $\theta$, thereby suggesting that transcriptional feedback could be a critical mechanism for facilitating entrainment of gene-expression networks.

# 4 Spectral theory for nonlinear networks

We now develop a framework to estimate the PSD for a general nonlinear network by applying Padé approximation theory which is known to be immensely useful in computing accurate rational function approximations for certain types of smooth non-linear functions. For any function $F$, a Padé approximant of order $m/n$ at some reference point $x_0$, is a ratio of two polynomials with numerator of degree $m$ and denominator of degree $n$, such that the values of the first $(m+n+1)$ derivatives (including the zeroth derivative) of the approximant match the corresponding derivatives of the function $F$ at $x_0$. Provided that the derivatives of the function $F$ can be computed, there exist an explicit expression to compute the required Padé approximant [44].

Recall the representation (2.8) of the autocovariance function which is equivalent to the representation (2.7) of the function $G(s)$ defined as in (2.6). Previous studies have established that usually the autocovariance function is well-approximated by only the first few terms in this infinite series. This fact can be justified by appealing to the compactness of the resolvent operator which ensures that it is close to a finite-rank operator. We shall use this property to approximate $G(s)$ with a finite sum of order $p$

$$G_p(s) = \sum_{j=1}^{p} \frac{\alpha_j}{s - \sigma_j}. \tag{4.24}$$

Applying the theory of Padé approximations, we come up with an efficient approach, called *Padé PSD*, to estimate this rational function and also certify its accuracy, using a single trajectory of the underlying CTMC.

Since functions $G$ and $G_p$ are complex-analytic, it suffices to identify $G_p$ on the positive real line. We can equivalently express $G_p$ as a rational function

$$G_p(s) := \frac{a_0 + a_1 s + \cdots + a_{p-1} s^{p-1}}{b_0 + b_1 s + \cdots + b_{p-1} s^{p-1} + s^p}. \tag{4.25}$$

Define functions $H$ and $H_p$ by $H(x) = x^{-1} G(x^{-1})$ and $H_p(x) = x^{-1} G_p(x^{-1})$. We shall infer $H_p(x)$ by estimating the order $(p-1)/p$ Padé approximant of the function $H(x)$ at $x = 0$. This also identifies the function $G_p(s)$ which can be viewed as order $(p-1)/p$ Padé approximant of the function $G(s)$ at $s = \infty$. It can be shown that for $m = 0, 1 \ldots, (2p-1)$, the $m$-th Padé derivative can be expressed as

$$D_m = \frac{1}{m!} \frac{\partial}{\partial x^m} H(x) \bigg|_{x=0} = \mathbb{E}_\pi \left( f \mathbb{A}^m f \right), \tag{4.26}$$

where the function $f$ is given by (2.5), and $\mathbb{A}^m$ denotes the $m$-th iterate of the generator $\mathbb{A}$ defined by (2.3). Observe that since $\mathbb{A}^0 = \mathbf{I}$ (the identity operator), the zeroth Padé derivative $D_0$ is simply the stationary variance $\text{Var}_\pi(X_n)$ which is also the total signal power (see Box 1).

Appealing to Birkhoff's Ergodic Theorem [58], we can estimate each Padé derivative $D_m$ from a single CTMC trajectory $(X(t))_{t \geq 0}$ by computing the long-term time-average of $\Psi_m(X(t))$ where $\Psi_m(x) = f(x) \mathbb{A}^m f(x)$. However this ergodic estimator is typically very slow to converge and hence we use stochastic analysis to design suitable covariates that can be added to this process to reduce the simulation time needed for convergence (see the Supplement, Section S2.4.2). This approach requires evaluations of functions of the form $\mathbb{A}^m f(x)$. This can be done recursively but it is computationally very intensive. In order to minimise

these evaluations we design a data structure that efficiently stores and retrieves the values of $\mathbb{A}^m f(x)$ for the states commonly visited by the trajectory. This allows us to leverage memory resources in order to improve computational performance and we utilise the property of ergodic Markov processes to repeatedly visit the same set of states.

Once the Padé derivatives $\widehat{D}_0, \ldots, \widehat{D}_{2p-1}$ have been estimated, the function $G_p$ can be easily identified by applying the Jacobi formula for Padé approximations [44]. Moreover in order to check if order $p$ approximation $G_p(s)$ accurately represents function $G(s)$, we compute a validity score based on direct estimations of the function $G(s)$ for certain $s$-values $s_1, \ldots, s_r$. These direct estimates can be obtained from the same CTMC trajectory that is generated to estimate the Padé derivatives, by augmenting the reaction network with $r$ species which keep track of the "history" of the output species state, at exponentially distributed random times in the past. Full theoretical and computational details of our Padé PSD method are provided in Sections S2.4 and S3 of the Supplement.

Our method is geared towards reaction networks that operate in the stochastic regime, due to constituent species having low copy-numbers. One way to verify that stochastic effects are indeed prominent is to check if the mixing strength (recall from Section 2.1) of the Markovian dynamics is high. This strength is difficult to quantify, but as [39] suggest, the ratio $\widehat{\rho} = -\widehat{D}_1/\widehat{D}_0$ is a good proxy for the mixing strength, because it provides an estimate of the Dirichlet form associated with the generator $\mathbb{A}$ (see [39]). Hence our method is more efficient when $\widehat{\rho} \gg 0$. In such a scenario we often find that the second order Padé approximant $G_2(s)$ is sufficient to accurately describe the function $G(s)$ and this observation has also been made in experimental studies [17]. We now provide an explicit expression for $G_2(s)$ in terms of the estimated Padé derivatives $\widehat{D}_0, \ldots, \widehat{D}_3$, and find a condition that characterises the existence of a maximum for the PSD at some positive frequency value $\omega_{\max}$. If such a maximum exists then it implies that the stochastic dynamics exhibits sustained oscillations with the dominant frequency of $\omega_{\max}$.

Letting

$$\delta_1 = \left( \frac{\widehat{D}_0\widehat{D}_3 - \widehat{D}_1\widehat{D}_2}{\widehat{D}_0\widehat{D}_2 - \widehat{D}_1^2} \right) \quad \text{and} \quad \delta_2 = \left( \frac{\widehat{D}_1\widehat{D}_3 - \widehat{D}_2^2}{\widehat{D}_0\widehat{D}_2 - \widehat{D}_1^2} \right),$$

the second order Padé approximant is given by

$$G_2(s) = \frac{\widehat{D}_0 s + \widehat{D}_1 - \delta_1 \widehat{D}_0}{s^2 - \delta_1 s + \delta_2}. \tag{4.27}$$

Equivalently we can express $G_2(s)$ in the form of (4.24) with coefficients $\alpha_1, \alpha_2$ and eigenvalues $\sigma_1, \sigma_2$ given by

$$\alpha_{1,2} = \frac{1}{2}\left[ \widehat{D}_0 \mp \left( \frac{2\widehat{D}_1 - \widehat{D}_0\delta_1}{\sqrt{\delta_1^2 - 4\delta_2}} \right) \right]$$
$$\text{and } \sigma_{1,2} = \frac{1}{2}\left[ \delta_1 \mp \sqrt{\delta_1^2 - 4\delta_2} \right].$$

Note that if $\delta_1^2 < 4\delta_2$ then the eigenvalues are complex conjugates of each other with non-zero imaginary parts. Applying (2.6) with $G(s) = G_2(s)$ we obtain the approximate PSD as

$$S_{X_n}(\omega) = -2\left( \frac{\delta_2(\widehat{D}_0\delta_1 - \widehat{D}_1) + \omega^2 \widehat{D}_1}{\delta_2^2 + (\delta_1^2 - 2\delta_2)\omega^2 + \omega^4} \right). \tag{4.28}$$

We now state a simple proposition that examines the conditions for stable oscillations to arise if the second order Padé approximant is accurate. The proof is provided in Section S2.4.3 of the Supplement.

**Proposition 4.1 (Oscillation conditions)** *Suppose $G(s) = G_2(s)$ and let $\delta_j$, $\alpha_j$ and $\sigma_j$ be defined as above for $j = 1, 2$. Then the PSD $S_{X_n}(\omega)$ achieves a local maximum at a non-zero frequency if and only if*

$$\delta_1^2 < 4\delta_2 \quad \textit{and} \quad \delta_2 > \frac{\beta\delta_1^2}{2\beta + 1}, \tag{4.29}$$

*where* $\beta = (\widehat{D}_0\delta_1 - \widehat{D}_1)/\widehat{D}_1$. *Such a maximum is also a global maximum for* $\omega \in [0, \infty)$ *and its location is given by*

$$\omega_{\max} = \sqrt{\beta\delta_2}\sqrt{-1 + \sqrt{1 + \frac{1}{\beta^2}\left[1 - \beta\left(\frac{\delta_1^2 - 2\delta_2}{\delta_2}\right)\right]}}. \tag{4.30}$$

## 4.1 Applications of the nonlinear theory

We now present applications of our Padé PSD method. First we reconsider the linear networks shown in Figure 3 where analytical expressions for the function $G(s)$ can be evaluated and compared to the Padé approximant produced by our method. The results are shown in Table 1 and one can see that the estimated Padé approximant is "close" to the analytical expression which is also reflected in the accuracy of our PSD estimation approach (see Figure 3).

| Network | Padé PSD $G_p(s)$ | Analytical $G(s)$ |
|---|---|---|
| Gene Expression | $\frac{1962.2s+2478.3}{s^2+1.4672s+0.47}$ | $\frac{1866.67s+2400}{s^2+1.5s+0.5}$ |
| RNA Splicing | $\frac{2.31s^2+13.42s+17.79}{s^3+6.18s^2+10.02s+3.64}$ | $\frac{2.37s^2+14.48s+20.28}{s^3+6.5s^2+11s+4}$ |
| IFF | $\frac{269.30s+166.58}{s^2+0.8039s+0.1506}$ | $\frac{266.67s+163.33}{s^2+0.8s+0.15}$ |
| NFB | $\frac{265.24s+272.14}{s^2+1.5285s+1.5282}$ | $\frac{266.67s+266.67}{s^2+1.5s+1.5}$ |

Table 1: The function $G(s)$ computed analytically and its Padé approximant $G_p(s)$ estimated with the Padé PSD method for the linear networks considered in Figure 3. The order of Padé approximation is 3 for the RNA Splicing network and it is 2 for all the other networks.

Next we provide two case studies to illustrate the usefulness of our PSD estimation method for synthetic biology applications. In the first study we examine the problem of optimising the oscillation strength of the *repressilator* [28] and in the second study we consider the problem of reducing oscillations at the single-cell level that typically arise due to the recently proposed *antithetic integral feedback* (AIF) controller [14] that has the important property of ensuring robust perfect adaptation for arbitrary intracellular networks with stochastic dynamics. In the rest of this section, we fix the order of approximation as two for the Padé PSD method.

### 4.1.1 Improving oscillation strength for the *repressilator*

The *repressilator* [28] is the first synthetic genetic oscillator and it consists of three genes repressing each other in a cyclic fashion (see Figure 5(A)). These three genes are *tetR* (from the Tn10 transposon), *cI* from bacteriophage $\lambda$ and *lacI* from the lactose operon. These three genes create three repressor proteins which are TetR, cI and LacI respectively, and the cyclic repression mechanism can be represented as

$$\text{TetR} \dashv \text{cI} \dashv \text{LacI} \dashv \text{TetR}.$$

Due to intrinsic noise in the dynamics, the *repressilator* loses oscillations at the bulk or population-average level after a few generations. At the single-cell level this intrinsic noise broadens the output PSD peak, making the oscillations less regular in both amplitude and phase. This issue was addressed in a recent paper [62] which elaborately studied the various sources of noise in the original circuit and eliminated them to construct a modified *repressilator* circuit that showed regular oscillations over several generations. It was found that most of the noise was generated when TetR protein levels are low and the derepression of the TetR controlled promoter occurs at low threshold. To raise this threshold a *sponge* plasmid was introduced and this had a remarkable effect of regularising the oscillations and sharpening the single-cell PSD peak.

Using the stochastic model given in the Supplement of [62] we demonstrate how our method is able to accurately estimate the single-cell PSD and exhibit the sharpening of the PSD in the presence of sponge. Our method also confirms that apart from using the sponge plasmid, the problem of low derepression threshold

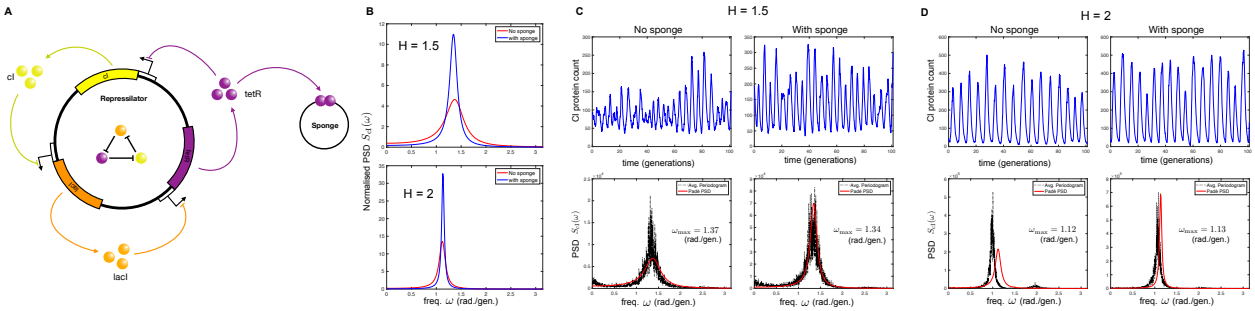


Figure 5: **Improving the *repressilator*'s oscillatory strength:** (A) Depiction of the *repressilator* network with three gene-expression systems whose output proteins cyclically repress each other. When present, the *sponge* plasmid can bind TetR proteins, thereby raising the derepression threshold of the *cI* gene. (B) Shows the effect of the sponge in sharpening the normalised PSD (PSD divided by the total signal power). This effect is seen both for promoter cooperativity $H = 1.5$ and $H = 2$, but the effect is more prominent in the former case. (C) Plots the single-cell trajectories with and without the sponge for promoter cooperativity $H = 1.5$, and it clearly shows that oscillations are more regular in the latter case. Comparison of the PSD estimated with our Padé PSD method with the PSDs estimated with the averaged periodogram method is provided and the location of the local maxima $\omega_{\max}$, as computed by (4.30), is shown. (D) Repeats the computational analysis in part (C) for promoter cooperativity $H = 2$.

can also be mitigated by designing promoters with a more cooperative repressor binding mechanism. The stochastic model is detailed in Section S4.2.1 of the Supplement. The repression mechanism is encoded with a nonlinear Hill function whose coefficient $H$ represents the degree of cooperativity among the promoter binding sites. The sponge plasmid, if present, can competitively bind the free TetR molecules, reducing the number of these molecules available for repressing the *cI* gene.

We use our method to estimate the PSD for the dynamics of the copy-numbers of the cI protein, whose expression is directly repressed by TetR. With second order Padé approximant, the normalised PSD (i.e. PSD divided by the total signal power) indeed exhibits a sharper peak at the peak frequency of around $\omega_{\max} \approx 1.35$ rad./gen. (see Figure 5(B)). This sharpness in PSD suggests more regularity in oscillations which is also evident from the single-cell trajectories plotted in Figure 5(C). We compare our PSD estimation method with the averaged periodogram approach in both the cases (with and without sponge) and the results are shown in Figure 5(C). Next we increased the promoter cooperativity (i.e. the Hill coefficient) from $H = 1.5$ to $H = 2$ and repeated the same analysis. The results indicate that when cooperativity is increased, the beneficial effect of the sponge in regularising the oscillations diminishes (see Figure 5(B,D)). This is because increased cooperativity makes the repression mechanism more ultrasensitive (see [35]) thereby increasing the derepression threshold even without the sponge plasmid. Notice that the PSDs obtained in this case with the averaged periodogram method show two distinct peaks - there is a major peak around frequency $\omega = 1$ rad./gen. and a minor peak at roughly twice this frequency. This effect is more prominent for the 'no sponge' case and the second minor peak is not captured by our second order Padé approximation. The existence of this second peak at twice the frequency of the first was first studied in [73] with CLE approximation of the dynamics, and it arises because the stochastic dynamics is close to the deterministic dynamics which exhibits oscillations due to a Hopf Bifurcation. In such cases the assumption of stationarity is violated for the considered simulation time and this makes our PSD estimation method error prone. We discuss this issue in Section S5 of the Supplement.

### 4.1.2 Reducing single-cell oscillations due to the antithetic integral feedback controller

In recent years genetic engineering has allowed researchers to implement bio-molecular control systems within living cells (see [14, 16, 64, 66, 4, 48, 42, 21, 43, 1, 5]). This area of research, popularly known as *Cybergenetics* [16], offers promise in enabling control of living cells for applications in biotechnology [75, 25] and therapeutics [77]. A particularly important challenge in Cybergenetics is to engineer an intracellular controller that facilitates cellular homeostasis by achieving *robust perfect adaptation* (RPA) for an output state-variable in an arbitrary intracellular stochastic reaction network. This challenge was theoretically

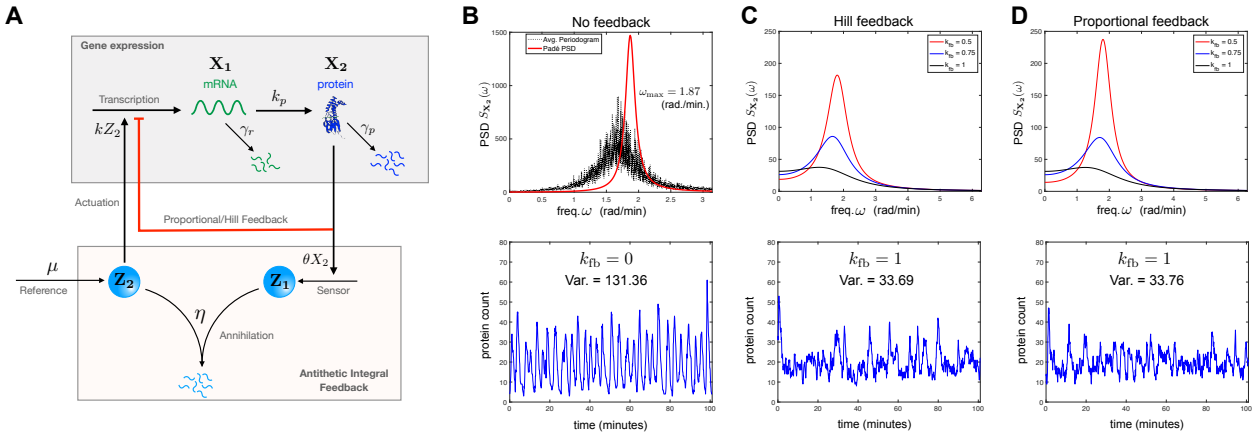


Figure 6: (A) Depiction of the bio-molecular *antithetic integral feedback* (AIF) controller regulating the gene-expression network. Here mRNA ($\mathbf{X_1}$) is the actuated species and the protein ($\mathbf{X_2}$) is the output species. This protein output is sensed by the controller species $\mathbf{Z_2}$ which annihilates the other controller species $\mathbf{Z_1}$ that is constitutively produced at rate $\mu$. The species $\mathbf{Z_1}$ actuates the gene-expression network by catalysing the production of mRNA $\mathbf{X_1}$. The red arrow indicates an extra negative feedback from the output species (protein) to the actuated species (mRNA). In (B) the single-cell oscillatory trajectory for the protein counts (without the extra feedback) is plotted and the corresponding PSD is estimated with Padé PSD and the averaged periodogram method. (C) Compares the PSDs estimated with the Padé PSD method for the Hill feedback for three choices of feedback parameter $k_{\rm fb}$. The single-cell trajectory for $k_{\rm fb} = 1$ min$^{-1}$ is plotted. (D) The computational analysis in part (C) is repeated for the proportional feedback. The plots for the single-cell trajectories also indicate the total signal power which is equal to the stationary output variance (see Box 1).

addressed in [14] which introduced the *antithetic integral feedback* (AIF) controller and demonstrated its ability to achieve RPA for the population-mean of output species. This controller has been synthetically implemented *in vivo* in bacterial cells, and it has been shown that any bio-molecular controller that achieves RPA for arbitrary reaction networks with noisy dynamics, must embed this controller [5].

Computational analysis has revealed that AIF controller can cause high-amplitude oscillations in the single-cell dynamics in certain parameter regimes [14, 60] which could potentially be undesirable and/or unfavorable. Hence it is important to find ways to augment the AIF controller, so that single-cell oscillations are attenuated but the RPA property is preserved. It is known that adding an extra negative feedback from the output species to the actuated species maintains the RPA property, while decreasing both the output variance and the settling-time for the mean dynamics [15]. Using the PSD estimation method developed in this paper we now demonstrate how adding such a negative feedback also helps in diminishing single-cell oscillations.

The AIF controller is depicted in Figure 6(A) and it is acting on the gene-expression model considered in Section 3.2.2. The AIF controller robustly steers the mean copy-number level of the protein $\mathbf{X_2}$ to the desired set-point $\mu/\theta$, where $\mu$ is the production rate of $\mathbf{Z_1}$ and $\theta$ is the reaction rate constant for the output sensing reaction. The AIF affects the output by actuating the production of mRNA $\mathbf{X_1}$ and the feedback loop is closed by the annihilation reaction between $\mathbf{Z_1}$ and $\mathbf{Z_2}$. This annihilation reaction can be viewed as mutual inactivation or sequestration and it can be realised using bio-molecular pairs such as sigma/anti-sigma factors [22, 52, 4], scaffold/anti-scaffold proteins [41] or toxin/antitoxin proteins [26].

It is known from [14] that the combined closed-loop dynamics is ergodic and mean steady-state protein copy-number is $\mu/\theta$

$$\lim_{t\to\infty} \mathbb{E}(X_2(t)) = \frac{\mu}{\theta}.$$

As discussed in [15], this ergodicity is preserved under certain conditions when an extra negative feedback reaction from protein $\mathbf{X_2}$ to mRNA $\mathbf{X_1}$ is added. Letting $z_1$ and $x_2$ denote the copy-numbers of $\mathbf{Z_1}$ and $\mathbf{X_2}$ respectively, we add the extra feedback by changing the rate of the actuation reaction from $kz_1$ to $(kz_1 + F_b(x_2))$ where $F_b$ is a monotonically decreasing feedback function which takes non-negative values.

As in [15] we consider two types of feedback. Letting $\widehat{\mu}$ to be the reference point, the first is Hill feedback of the form

$$F_b(x_2) = \frac{4k_{\text{fb}}\widehat{\mu}^2}{\widehat{\mu} + x_2}$$

which is based on the actual output copy-number $x_2$, while the second is the *proportional* feedback that is essentially the linearisation of the Hill feedback at the reference point $\widehat{\mu}$

$$F_b(x_2) = k_{\text{fb}} \max\{3\widehat{\mu} - x_2, 0\}.$$

One can easily see that at the reference point, the values of this feedback function $F_b(\widehat{\mu})$ and its derivative $F_b'(\widehat{\mu})$ (equal to $-k_{\text{fb}}$) are the same for both types of feedback. We can view $k_{\text{fb}}$ as the feedback gain parameter. The Hill feedback is biologically more realisable, while the proportional feedback captures the classical controller where the feedback strength depends linearly on the deviation of the output $x_2$ from the reference point $\widehat{\mu}$, in the output range $[0, 3\widehat{\mu}]$. In our analysis we set the reference point $\widehat{\mu}$ as the set-point $\mu/\theta$.

For a particular network parametrization we use our method to estimate the PSD for the single-cell protein dynamics in the AIF regulated gene-expression network, and the results are displayed in Figure 6. When the extra negative feedback is absent (i.e. $k_{\text{fb}} = 0$) the single-cell trajectory has high-amplitude oscillations which is also evident from the estimated PSD (see Figure 6(B)). In Figure 6 (C) we apply our Padé PSD method to examine how the PSD changes when extra feedback of Hill type is added with varying strengths given by parameter $k_{\text{fb}}$. Observe that as the feedback strength increases, the PSD peak declines and the the oscillations become almost non-existent for $k_{\text{fb}} = 1$ min$^{-1}$. The same holds true for the proportional feedback (see Figure 6(D)). These results suggest that both feedback mechanisms are more or less equally effective in reducing oscillations. This is further corroborated by the single-cell trajectories plotted in Figure 6(C-D) which also shows that addition of feedback decreases the stationary output variance, that is equal to the signal power (see Box 1). The details on the computations for the AIF regulated gene-expression network can be found in Section S4.2.2 of the Supplement.

# 5 Discussion

Recent advances in microscopic imaging and fluorescent reporter technologies have enabled high-resolution monitoring of processes within living cells [57]. As the accessibility of this time-course data rapidly increases, there is an urgent need to design novel theoretical and computational approaches that make use of the full scope of such data, in order to understand intracellular processes and design effective synthetic circuits. An important feature of time-course measurements, which is lacking in the data generated by the more common experimental technique of Flow-Cytometry, is that they capture temporal correlations at the single-cell level which are rich in information about the underlying dynamical model. Frequency domain analysis provides a viable approach to extract this information, if we have an efficient framework to connect network models to the frequency spectrum or the power spectral density (PSD) of the single-cell trajectories measured with time-lapse microscopy [71, 24]. The dynamics within cells is invariably stochastic, owing to the presence of many low abundance biomolecular species, and it is commonly described as a continuous-time Markov chain (CTMC). In this context, the aim of this paper is to develop an analytical and computational method for reliably estimating the PSD for single-cell trajectories from CTMC models. Existing approaches for PSD estimation for stochastic network models, are either applicable to a particular class of networks [70, 68], or they are based on dynamical approximations that are known to be inaccurate over large time-intervals and in situations where low abundance species are present [71, 69]. Our method does not suffer from these drawbacks. It applies generically to any stable network and it yields an accurate PSD expression using a single simulation of the CTMC trajectory. Moreover for networks with affine propensity functions we provide an exact expression for the PSD.

The tools we develop in this paper are of significance to both systems and synthetic biology. We demonstrate that in the presence of intrinsic noise, PSD estimation can successfully differentiate between adapting Incoherent Feedforward (IFF) and Negative Feedback (NFB) topologies [53], and it can facilitate performance optimisation of synthetic oscillators [28] as well as synthetic *in vivo* controllers [14]. Moreover it

can also aid the study of stochastic entrainment at the single-cell level. This is of particular relevance for applications such as designing pulsatile dynamics of transcription factors, which is known to enable graded multi-gene regulation [8].

One of the main contributions of this paper is to show how the theory of Padé approximations can be effectively applied to the PSD estimation problem for reaction networks with stochastic CTMC dynamics. In our method a low dimensional approximation of the PSD is computed based on estimates of Padé derivatives that are expressible as stationary expectations of certain functions involving the observable output and its image under iterations of the CTMC generator. These ideas can be combined with several existing techniques to significantly improve the efficiency of our PSD estimation method. Specifically the problem of reliably estimating expectations of functions under the CTMC model has received a lot of attention in recent years [76], and methods designed for this problem, like $\tau$-leaping [19] and/or multilevel schemes [3], can be easily integrated with our framework. Moreover model reduction [46, 40] and simulation tools [18, 27] for multiscale networks can be readily applied to simplify the estimation of Padé derivatives. The main bottleneck in the estimation of these derivatives is the cumbersome recursive computation of the iterates of the CTMC generator. Modern computer algebra systems [56] may provide a viable alternative to this recursive approach and this would go a long way in reducing the required computational time.

**Acknowledgements:** This project has received funding from the European Research Council (ERC) under the European Union's Horizon 2020 research and innovation programme grant agreement no. 743269 (CyberGenetics project).

# References

[1] D. K. Agrawal, R. Marshall, V. Noireaux, and E. D. Sontag. In vitro implementation of robust gene regulation in a synthetic biomolecular integral controller. *bioRxiv*, page 525279, 2019. 4.1.2

[2] D. Anderson and T. Kurtz. Continuous time Markov chain models for chemical reaction networks. In H. Koeppl, G. Setti, M. di Bernardo, and D. Densmore, editors, *Design and Analysis of Biomolecular Circuits*. Springer-Verlag, 2011. 1, 2.1, 2.1

[3] D. F. Anderson and D. J. Higham. Multilevel monte carlo for continuous time markov chains, with applications in biochemical kinetics. *Multiscale Modeling & Simulation*, 10(1):146–179, 2012. 5

[4] F. Annunziata, A. Matyjaszkiewicz, G. Fiore, C. S. Grierson, L. Marucci, M. di Bernardo, and N. J. Savery. An orthogonal multi-input integration system to control gene expression in escherichia coli. *ACS synthetic biology*, 6(10):1816–1824, 2017. 4.1.2, 4.1.2

[5] S. K. Aoki, G. Lillacci, A. Gupta, A. Baumschlager, D. Schweingruber, and M. Khammash. A universal biomolecular integral feedback controller for robust perfect adaptation. *Nature*, 570(7762):533–537, 2019. 4.1.2

[6] A. P. Arkin, C. V. Rao, and D. M. Wolf. Control, exploitation and tolerance of intracellular noise. *Nature*, 420:231–237, 2002. 1

[7] N. Bagheri, S. R. Taylor, K. Meeker, L. R. Petzold, and F. J. Doyle III. Synchrony and entrainment properties of robust circadian oscillators. *Journal of The Royal Society Interface*, 5(suppl_1):S17–S28, 2008. 3.2.5

[8] D. Benzinger and M. Khammash. Pulsatile inputs achieve tunable attenuation of gene expression variability and graded multi-gene regulation. *Nature communications*, 9(1):1–10, 2018. 5

[9] V. Bergen, M. Lange, S. Peidli, F. A. Wolf, and F. J. Theis. Generalizing rna velocity to transient cell states through dynamical modeling. *Nature Biotechnology*, pages 1–7, 2020. 3.2, 3.2.3

[10] C. Beta and K. Kruse. Intracellular oscillations and waves. *Annual Review of Condensed Matter Physics*, 8:239–264, 2017. 3.2.5

[11] O. Borkowski, F. Ceroni, G.-B. Stan, and T. Ellis. Overloaded and stressed: whole-cell considerations for bacterial synthetic biology. *Current opinion in microbiology*, 33:123–130, 2016. 1

[12] D. Bratsun, D. Volfson, L. S. Tsimring, and J. Hasty. Delay-induced stochastic oscillations in gene regulation. *Proceedings of the National Academy of Sciences*, 102(41):14593–14598, 2005. 1

[13] C. Brezinski and J. Van Iseghem. Padé approximations. *Handbook of Numerical Analysis*, 3:47–222, 1994. 1

[14] C. Briat, A. Gupta, and M. Khammash. Antithetic integral feedback ensures robust perfect adaptation in noisy biomolecular networks. *Cell systems*, 2(1):15–26, 2016. 1, 4.1, 4.1.2, 4.1.2, 5

[15] C. Briat, A. Gupta, and M. Khammash. Antithetic proportional-integral feedback for reduced variance and improved control performance of stochastic reaction networks. *Journal of The Royal Society Interface*, 15(143):20180079, 2018. 4.1.2, 4.1.2

[16] C. Briat, C. Zechner, and M. Khammash. Design of a synthetic integral feedback circuit: dynamic analysis and dna implementation. *ACS synthetic biology*, 5(10):1108–1116, 2016. 4.1.2

[17] L. Cai, C. K. Dalal, and M. B. Elowitz. Frequency-modulated nuclear localization bursts coordinate gene regulation. *Nature*, 455(7212):485–490, 2008. 4

[18] Y. Cao, D. Gillespie, and L. Petzold. The slow-scale stochastic simulation algorithm. *Journal of Chemical Physics*, 122(1):1–18, 2005. 5

[19] Y. Cao, D. T. Gillespie, and L. R. Petzold. Efficient step size selection for the tau-leaping simulation method. *The Journal of Chemical Physics*, 124(4), 2006. 5

[20] Z. Cao and R. Grima. Linear mapping approximation of gene regulatory networks with stochastic dynamics. *Nature communications*, 9(1):1–15, 2018. 1

[21] F. Ceroni, A. Boo, S. Furini, T. E. Gorochowski, O. Borkowski, Y. N. Ladak, A. R. Awan, C. Gilbert, G.-B. Stan, and T. Ellis. Burden-driven feedback control of gene expression. *Nature methods*, 15(5):387, 2018. 4.1.2

[22] D. Chen and A. P. Arkin. Sequestration-based bistability enables tuning of the switching boundaries and design of a latch. *Molecular systems biology*, 8(1):620, 2012. 4.1.2

[23] J. W. Cooley and J. W. Tukey. An algorithm for the machine calculation of complex fourier series. *Mathematics of computation*, 19(90):297–301, 1965. 1

[24] C. D. Cox, J. M. McCollum, D. W. Austin, M. S. Allen, R. D. Dar, and M. L. Simpson. Frequency domain analysis of noise in simple gene circuits. *Chaos: An Interdisciplinary Journal of Nonlinear Science*, 16(2):026102, 2006. 1, 5

[25] B. F. Cress, E. A. Trantas, F. Ververidis, R. J. Linhardt, and M. A. Koffas. Sensitive cells: enabling tools for static and dynamic control of microbial metabolic pathways. *Current opinion in biotechnology*, 36:205–214, 2015. 4.1.2

[26] N. De Jonge, A. Garcia-Pino, L. Buts, S. Haesaerts, D. Charlier, K. Zangger, L. Wyns, H. De Greve, and R. Loris. Rejuvenation of ccdb-poisoned gyrase by an intrinsically disordered protein domain. *Molecular cell*, 35(2):154–163, 2009. 4.1.2

[27] W. E, D. Liu, and E. Vanden-Eijnden. Nested stochastic simulation algorithms for chemical kinetic systems with multiple time scales. *J. Comput. Phys.*, 221(1):158–180, Jan. 2007. 5

[28] M. B. Elowitz and S. Leibler. A synthetic oscillatory network of transcriptional regulators. *Nature*, 403(6767):335–338, 2000. 1, 4.1, 4.1.1, 5

[29] S. Engelberg. *Digital signal processing: an experimental approach*. Springer Science & Business Media, 2008. 1, 1

[30] S. N. Ethier and T. G. Kurtz. *Markov processes : Characterization and Convergence*. Wiley Series in Probability and Mathematical Statistics: Probability and Mathematical Statistics. John Wiley & Sons Inc., New York, 1986. 2.1

[31] P. J. Fraker, L. E. King, D. Lill-Elghanian, and W. G. Telford. Quantification of apoptotic events in pure and heterogeneous populations of cells using the flow cytometer. In *Methods in cell biology*, volume 46, pages 57–76. Elsevier, 1995. 1

[32] N. Geva-Zatorsky, E. Dekel, E. Batchelor, G. Lahav, and U. Alon. Fourier analysis and systems identification of the p53 feedback loop. *Proceedings of the National Academy of Sciences*, 107(30):13550–13555, 2010. 1

[33] D. T. Gillespie. Exact stochastic simulation of coupled chemical reactions. *The Journal of Physical Chemistry*, 81(25):2340–2361, 1977. 2.1

[34] D. T. Gillespie. The chemical langevin equation. *The Journal of Chemical Physics*, 113(1):297–306, 2000. 1

[35] A. Goldbeter and D. E. Koshland. An amplified sensitivity arising from covalent modification in biological systems. *Proceedings of the National Academy of Sciences*, 78(11):6840–6844, 1981. 4.1.1

[36] J. Goutsias. Classical versus stochastic kinetics modeling of biochemical reaction systems. *Biophysical Journal*, 92(7):2350–2365, 2007. 1

[37] A. Gupta, C. Briat, and M. Khammash. A scalable computational framework for establishing long-term behavior of stochastic reaction networks. *PLoS Comput Biol*, 10(6):e1003669, 06 2014. 2.1, 3

[38] A. Gupta and M. Khammash. Computational identification of irreducible state-spaces for stochastic reaction networks. *SIAM Journal on Applied Dynamical Systems*, 17(2):1213–1266, 2018. 2.1

[39] A. Gupta, A. Milias-Argeitis, and M. Khammash. Dynamic disorder in simple enzymatic reactions induces stochastic amplification of substrate. *Journal of The Royal Society Interface*, 14(132):20170311, 2017. 4

[40] B. Hepp, A. Gupta, and M. Khammash. Adaptive hybrid simulations for multiscale stochastic reaction networks. *The Journal of chemical physics*, 142(3):034118, 2015. 5

[41] V. Hsiao, E. L. De Los Santos, W. R. Whitaker, J. E. Dueber, and R. M. Murray. Design and implementation of a biomolecular concentration tracker. *ACS synthetic biology*, 4(2):150–161, 2014. 4.1.2

[42] V. Hsiao, A. Swaminathan, and R. M. Murray. Control theory for synthetic biology: Recent advances in system characterization, control design, and controller implementation for synthetic biology. *IEEE Control Systems Magazine*, 38(3):32–62, 2018. 4.1.2

[43] H.-H. Huang, Y. Qian, and D. Del Vecchio. A quasi-integral controller for adaptation of genetic modules to variable ribosome demand. *Nature communications*, 9(1):5415, 2018. 4.1.2

[44] C. G. J. Jacobi. Über die darstellung einer reihe gegebner werthe durch eine gebrochne rationale function. *Journal für die reine und angewandte Mathematik*, 30:127–156, 1846. 4, 4

[45] C. Jia, M. Q. Zhang, and H. Qian. Analytic theory of stochastic oscillations in single-cell gene expression. *arXiv preprint arXiv:1909.09769*, 2019. 1, 3.2.4

[46] H.-W. Kang and T. G. Kurtz. Separation of time-scales and model reduction for stochastic reaction networks. *Ann. Appl. Probab.*, 23(2):529–583, 2013. 5

[47] T. Kato. *Perturbation theory for linear operators*, volume 132. Springer Science & Business Media, 2013. 1

[48] C. L. Kelly, A. W. K. Harris, H. Steel, E. J. Hancock, J. T. Heap, and A. Papachristodoulou. Synthetic negative feedback circuits using engineered small rnas. *Nucleic acids research*, 46(18):9875–9889, 2018. 4.1.2

[49] T. B. Kepler and T. C. Elston. Stochasticity in transcriptional regulation: Origins, consequences, and mathematical representations. *Biophysical Journal*, 81(6):3116 – 3136, 2001. 1

[50] A. Khintchine. Korrelationstheorie der stationären stochastischen prozesse. *Mathematische Annalen*, 109(1):604–615, 1934. 1

[51] T. G. Kurtz. Strong approximation theorems for density dependent markov chains. *Stochastic Processes and their Applications*, 6(3):223–240, 1978. 1

[52] G. Lillacci, S. K. Aoki, D. Schweingruber, and M. Khammash. A synthetic integral feedback controller for robust tunable regulation in bacteria. *BioRxiv*, page 170951, 2017. 4.1.2

[53] W. Ma, A. Trusina, H. El-Samad, W. A. Lim, and C. Tang. Defining network topologies that can achieve biochemical adaptation. *Cell*, 138(4):760–773, 2009. 1, 3.2, 5

[54] H. H. McAdams and A. Arkin. Stochastic mechanisms in gene expression. *Proc. Natl. Acad. Sci., Biochemistry*, 94:814–819, 1997. 1

[55] A. J. McKane, J. D. Nagy, T. J. Newman, and M. O. Stefanini. Amplified biochemical oscillations in cellular systems. *Journal of Statistical Physics*, 128(1-2):165–191, 2007. 1

[56] A. e. a. Meurer. Sympy: symbolic computing in python. *PeerJ Computer Science*, 3:e103, Jan. 2017. 5

[57] D. Mullassery, C. A. Horton, C. D. Wood, and M. R. White. Single live cell imaging for systems biology. *Essays in biochemistry*, 45:121, 2008. 1, 5

[58] J. R. Norris. *Markov chains*, volume 2 of *Cambridge Series in Statistical and Probabilistic Mathematics*. Cambridge University Press, Cambridge, 1998. Reprint of 1997 original. 4

[59] H. Nyquist. Certain topics in telegraph transmission theory. *Transactions of the American Institute of Electrical Engineers*, 47(2):617–644, 1928. 1

[60] N. Olsman, F. Xiao, and J. C. Doyle. Architectural principles for characterizing the performance of antithetic integral feedback networks. *iScience*, 14:277–291, 2019. 4.1.2

[61] A. Pikovsky, J. Kurths, M. Rosenblum, and J. Kurths. *Synchronization: a universal concept in nonlinear sciences*, volume 12. Cambridge university press, 2003. 3.2.5

[62] L. Potvin-Trottier, N. D. Lord, G. Vinnicombe, and J. Paulsson. Synchronous long-term oscillations in a synthetic gene circuit. *Nature*, 538(7626):514–517, 2016. 4.1.1

[63] J. E. Purvis and G. Lahav. Encoding and decoding cellular information through signaling dynamics. *Cell*, 152(5):945–956, 2013. 3.2.5

[64] Y. Qian and D. Del Vecchio. Realizing 'integral control' in living cells: how to overcome leaky integration due to dilution? *Journal of The Royal Society Interface*, 15(139):20170902, 2018. 4.1.2

[65] H. Risken. Fokker-planck equation. In *The Fokker-Planck Equation*, pages 63–95. Springer, 1996. 3

[66] C. C. Samaniego and E. Franco. An ultrasensitive biomolecular network for robust feedback control. *IFAC-PapersOnLine*, 50(1):10950–10956, 2017. 4.1.2

[67] N. C. Shaner, P. A. Steinbach, and R. Y. Tsien. A guide to choosing fluorescent proteins. *Nature methods*, 2(12):905–909, 2005. 1

[68] M. L. Simpson, C. D. Cox, and G. S. Sayler. Frequency domain analysis of noise in autoregulated gene circuits. *Proceedings of the National Academy of Sciences*, 100(8):4551–4556, 2003. 1, 5

[69] M. L. Simpson, C. D. Cox, and G. S. Sayler. Frequency domain chemical langevin analysis of stochasticity in gene transcriptional regulation. *Journal of theoretical biology*, 229(3):383–394, 2004. 1, 3.1, 5

[70] S. Song, G.-S. Yang, S. J. Park, S. Hong, J.-H. Kim, and J. Sung. Frequency spectrum of chemical fluctuation: A probe of reaction mechanism and dynamics. *PLoS computational biology*, 15(9):e1007356, 2019. 1, 1, 5

[71] S. Tănase-Nicola, P. B. Warren, and P. R. Ten Wolde. Signal detection, modularity, and the correlation between extrinsic and intrinsic noise in biochemical networks. *Physical review letters*, 97(6):068102, 2006. 1, 1, 3.1, 5

[72] M. Thattai and A. Van Oudenaarden. Intrinsic noise in gene regulatory networks. *Proceedings of the National Academy of Sciences*, 98(15):8614–8619, 2001. 3.2

[73] P. Thomas, A. V. Straube, J. Timmer, C. Fleck, and R. Grima. Signatures of nonlinearity in single cell noise-induced oscillations. *Journal of theoretical biology*, 335:222–234, 2013. 1, 4.1.1

[74] N. G. van Kampen. A power series expansion of the master equation. *Canadian Journal of Physics*, 39(4):551–567, 1961. 1

[75] N. Venayak, N. Anesiadis, W. R. Cluett, and R. Mahadevan. Engineering metabolism through dynamic control. *Current opinion in biotechnology*, 34:142–152, 2015. 4.1.2

[76] D. J. Warne, R. E. Baker, and M. J. Simpson. Simulation and inference algorithms for stochastic biochemical reaction networks: from basic concepts to state-of-the-art. *Journal of the Royal Society Interface*, 16(151):20180943, 2019. 5

[77] H. Ye and M. Fussenegger. Synthetic therapeutic gene circuits in mammalian cells. *FEBS letters*, 588(15):2537–2544, 2014. 4.1.2